INSTITUTE OF PHYSICS PUBLISHING JOURNAL OF PHYSICS: CONDENSED MATTER

J. Phys.: Condens. Matter **18** (2006) 1175–1188 doi:10.1088/0953-8984/18/4/006

Multipolar emission in the vicinity of metallic nanostructures

P G Etchegoin and E C Le Ru

The MacDiarmid Institute for Advanced Materials and Nanotechnology, School of Chemical and Physical Sciences, Victoria University of Wellington, PO Box 600, Wellington, New Zealand

E-mail: Pablo.Etchegoin@vuw.ac.nz and Eric.LeRu@vuw.ac.nz

Received 2 August 2005
Published 9 January 2006
Online at stacks.iop.org/JPhysCM/18/1175

Abstract

Electromagnetic emission from finite-size multipoles very close to metal surfaces exhibiting plasmon resonances can have profound consequences on the characteristics of the emitted radiation in the far field in both its integrated intensity and its spatial distribution. The problem is relevant for many types of spectroscopies that use metals to enhance optical signals, but it also represents a complementary aspect to the recent interest in near-field imaging via surface plasmon resonances. The breakdown of selection rules for multipolar emission and the phenomenon of *radiation funnelling* in the far field are explicitly discussed. The relevance of these concepts for certain types of spectroscopy, like surface enhanced Raman scattering (SERS), is also highlighted.

(Some figures in this article are in colour only in the electronic version)

1. Introduction and overview

We aim at showing that multipolar radiation originating from objects with typical sizes comparable to molecules can be *activated* (in a way to be specified later), redirected, and detected, in the far field by the influence of surface plasmon resonances. This leads automatically to polarization selection rule breakdowns for certain types of spectroscopies like Raman scattering, but also leads to the study of *far-field funnelling* of the emitted radiation, a subject of prime importance for spectroscopic applications and complementary to a large extent to recent interests in near-field imaging by plasmon excitations.

We would like first to put the problem in a more general context as an overview and motivation for the discussions that follow in the subsequent sections. In the last decade, the interest in photonic crystals and light localization [1, 2] has fuelled an enormous amount of work at the interface between classical electrodynamics and highly disordered and/or metallic media [3]. There has been also renewed interest in the optical properties of random dielectric media [4] (to achieve light stimulation [5]) and in time-dependent optical phenomena where giant transient local fields have been predicted [6]. A sub-family of these problems deals specifically with metals and surface plasmon–polariton excitations in them. The field has grown

so vastly in the last few years that specific reviews on the nano-optics of surface plasmon–polaritons can be found in the literature [7].

Within the family of problems that deal specifically with the optical properties of metals in the nanometre-size range, there are different subfamilies that caught the attention of different groups. Many aspects are directly linked to spectroscopy and emission of radiation in the presence of surface plasmon excitations [8–11], a subject with a long-standing history in optics and spectroscopy [12, 13]. The concept that molecules can serve as direct probes of the near field [14] has been acknowledged and it is widely used in surface enhanced Raman spectroscopy (SERS) [13, 15, 16]. In addition, the more recent proposal of *perfect lensing* [17], and the possibility of manipulating the near field in useful ways has been added to the list [18]. The concept that the local evanescent fields of an emitting source can be amplified and refocused to reconstruct an image beyond the shortcomings of the diffraction limit has generated a great deal of controversy in the literature [19–21], and a wealth of theoretical and experimental work [22]. Pendry's idea of a super-lens [17] in the optical range is based on the effect of a metallic sheet on the evanescent field of an object at the wavelength λ where the dielectric function $\epsilon(\lambda)$ satisfies $\mathrm{Re}[\epsilon(\lambda)] \sim -1$, $\mathrm{Im}[\epsilon(\lambda)] \sim 0$, where Re and Im are the real and imaginary parts, respectively. It is known now that 'perfect lensing' can only exist with a resolution severely limited by residual absorption, with a logarithmic singularity that prevents super-resolution [23–25]. Still, it represents a useful concept that has had already some applications in photolithography [22].

This is where the problem we want to treat in this paper makes contact with the existing background activities. We believe that the emphasis on the effect of surface plasmons on the near field for the imaging problem has completely circumvented other effects on localized emission near metals which are, in fact, more relevant for spectroscopic applications. In particular, the study of the effect of plasmon resonances on the multipolar components of the emission and the nature of scattering cross sections under the presence of strong local fields and self-reactions. Imaging (even at a single wavelength like in the super-lens problem) is a more restricted problem than spectroscopy [26]. This is because the reconstruction of an image requires the handling and proper superposition of many *spatial* frequencies while the spectral content of an object can be measured even if its image is completely destroyed. We cannot see the image of a lamp through an opalescent glass, but we can measure its spectral content with no problem for as long as part of its radiation enters into the numerical aperture of a detecting system.

Accordingly, for reasons to do with potential spectroscopic applications where imaging is not an issue, it is interesting to understand the effect of nearby plasmon surface resonances on the bound and/or multipolar fields of an emitter, and in particular, the consequences for the far field, where most spectroscopic applications would take place. This is the subject of the present paper. We shall show through direct numerical simulation that surface plasmons can activate multipolar radiation components and make them a substantial fraction of (or comparable to) dipolar emission under certain circumstances. We shall also illustrate the phenomenon of *energy funnelling* in the far field which should be very important for spectroscopic applications. A few possible connections with experimentally observed phenomena (like Raman selection rule breakdowns in SERS) are also analysed. As a matter of fact, we introduce the problem and the reasons why it should be interesting to study it through concepts borrowed from Raman scattering in the bond-polarizability approach in the next section.

2. Bond-polarizability model and multipole radiation

The macroscopic theory of inelastic light scattering in solids and molecules leads to the so-called *bond-polarizability model* [27] of widespread use and success in molecular spectroscopy.

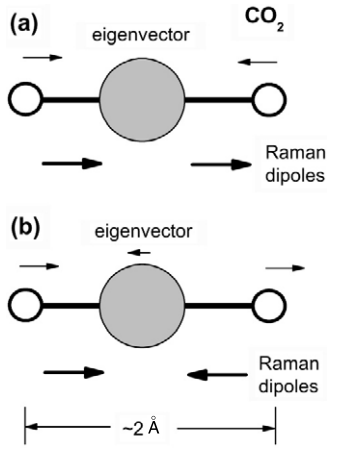

Figure 1. Two of the bond-stretching vibrational modes in CO_2 and their equivalent Raman dipoles in each bond. (a) shows a symmetric Raman active (IR inactive) stretching mode, while (b) is an asymmetric Raman inactive (IR active) bond-stretching vibration. Inactive Raman modes are interpreted, in the bond-polarizability model, as coming from the emission of finite-size higher-order multipoles. See the text for further details.

A bond-polarizability description of the scattering process, which was originally introduced by Placzek [28, 29] and later generalized for macromolecules by Volkenstein [30], is typically most successful for *covalent* bonds and has been widely justified by *ab initio* methods. In this picture, an individual bond has a linear optical polarizability tensor $\hat{\alpha}_{ij}$ which is changed by bond deformations (stretching or bending) produced by normal mode vibrations. The derivatives of $\hat{\alpha}_{ij}$ with respect to displacements define a new third-rank tensor, which—when contracted with the displacement vector of the bond deformation—defines the *Raman tensor* of the bond [27]. Hence, the total Raman tensor of a molecule is the sum of all individual bond tensors with their relative orientations accounted for. If the eigenvector of a mode is known, accordingly, the Raman tensor of that vibration can be obtained and will be a Raman active, inactive, or partially active mode depending on mutual cancellations of contributions according to symmetry.

In this picture, therefore, each bond acts as a small localized dipole oscillating at the phonon frequency, and re-emitting the Stokes shifted radiation. It is the coherent superposition of the radiation of all these dipoles which makes a mode Raman active or inactive in the far field. The textbook example is two of the modes of carbon dioxide, shown in figure 1. By considering only two modes with bond-stretching eigenvectors the problem becomes one dimensional and of easy analysis. The mode in figure 1(a) produces two bond contractions which are in phase and therefore the two Raman dipoles of the two bonds add constructively and are seen as a Raman active mode from the far field. The mode in figure 1(b), on the contrary, produces two out-of-phase Raman dipoles separated by a distance of $\sim$1 Å. This results then, formally, in quadrupolar emission and in a Raman forbidden mode. The mode in figure 1(b) is, in fact, infrared (IR) active and there is here a mutual exclusion with Raman active modes due to the presence of an inversion centre.

Under a plane wave excitation the situation is clear-cut: (i) there is no inhomogeneity in the excitation, (ii) typical molecular sizes are much smaller that the wavelength (λ), (iii) Raman dipoles will be excited in phase and with the same amplitude, and (iv) vibrations will be Raman active/inactive depending purely on the symmetry of the molecular structure.

In close proximity of surface plasmon excitations, however, huge field gradients varying over distances of nanometres or fractions of a nanometre are commonplace. This is, for example, the environment in which molecules emit sometimes their scattered radiation in SERS. There is a case, therefore, to study multipolar emissions from sources with typical molecular dimensions in close proximity to metals.

Through the study of a few specific examples we want to address the following questions: (i) can the multipolar nature of the emission be changed by the influence of surface plasmons? (ii) can the energy be redirected (funnelled) in specific directions? and (iii) can selection rules be broken? Some of these issues (in particular (i) and (ii)) have been partially discussed in [26] using a much simpler numerical algorithm (discrete dipole approximation, DDA [31–34]) for the electromagnetic calculation. Methods like the DDA, however, do not represent the local field well for sources very close to the metal particles ($\sim$1 nm) unless variable cell size discretization is used. Here we resort to direct numerical simulation of Maxwell's equations through finite element modelling. The examples given in the following sections address several aspects of the problems outlined above.

3. Multipolar radiation close to metallic structures

All simulations in this paper have been performed by direct numerical solutions of Maxwell's equations through finite elements with adaptive meshes [35–37]. To this end, we use modified Matlab[1] codes set up by FEMLAB (see footnote 1). For clarity and ease of representation of the fields we work in two-dimensional cases; this is not a limitation to the underlying concepts we would like to highlight here and simplifies enormously the visualization of the field distributions.

We choose to work in an electromagnetic 2D transverse magnetic (TM) problem. The basic setting of the problem is shown in figure 2. A bounding box of size $1 \times 1\ \mu\text{m}^2$ is set up with low reflecting (LR) boundaries to solve the emission problem of a localized source in the middle. LR boundaries are strictly non-reflecting only for plane waves [39], but they provide an excellent approximation for open boundaries in general if the size of the box is not too small compared to λ. Inside the bounding box, one or several metallic objects are placed together with the source which is built out of δ-like singularities in the transverse magnetic field H_z. The objects satisfy standard continuity conditions at the interfaces (specified in the figure) and the sources we shall study represent finite-size dipoles or quadrupoles with typical molecular dimensions. The δ-like singularities in H_z can be arranged in different ways to define different types of electric dipoles or quadrupoles (two δ-like singularities in H_z of opposite sign and in close proximity along x represent an electric dipole in the x–y plane polarized along y). Two examples are explicitly shown in figure 2. The angular pattern of intensity emission of the quadrupoles in figures 2(a) and (b) are shown in figure 2(c); they are calculated via the Poynting vector flux [38] across a circular boundary of radius 0.30 μm encircling the source[2]. Given the configuration of the δ-singularities, we call these quadrupoles the *square* (I_S) and *line* (I_L) quadrupoles; they are equivalent to two out-of-phase electric dipoles polarized along y and aligned in close proximity along the vertical axis for I_S; or aligned along the horizontal axis for I_L. Compared to an electric dipole created by only two δ-singularities in H_z, the intensity at

[1] All simulations in this paper were produced with Matlab [The MathWorks Inc. (www.mathworks.com)] with adaptive-mesh scripts for electromagnetic calculations generated by FEMLAB [Comsol Inc. (www.femlab.com)].

[2] The angular pattern of the Poynting vector along this circle will be a good approximation for as long as the circle is already in a region where the bound field has no influence. This can be judged by how radial the streamlines of the Poynting vector are. In some of our calculations this has an influence and the angular pattern we display is only an approximation to the far-field angular distribution.

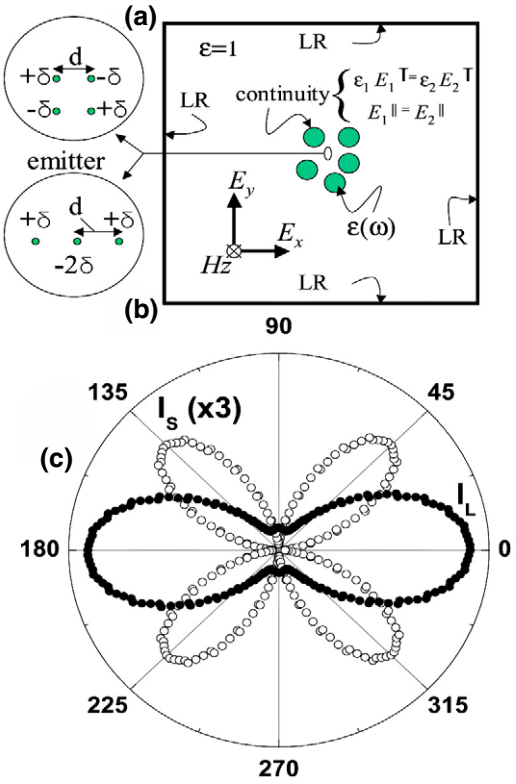

Figure 2. Top: basic geometry of the 2D TM problem. A box ($1 \times 1\ \mu\text{m}^2$) with low-reflectance (LR) boundaries [39] defines the region where Maxwell's equation for the perpendicular magnetic field H_z is solved (TM problem). Quadrupolar sources are built as collections of δ-singularities in H_z with different spatial configurations. The objects inside the box fulfill standard boundary conditions as specified in the figure. The blowouts of the source in (a) and (b) show two different types of quadrupoles (square: I_S and line: I_L quadrupoles) built from δ-like singularities in H_z. In (c) the polar plots of the emission of both quadrupoles in vacuum are shown on a linear scale.

the maximum of the lobe in I_L in figure 2(c) is $\sim 5 \times 10^{-6}$ times smaller at $\lambda = 500$ nm, which renders its intensity undetectable in the far field under normal conditions. Quadrupole radiation in the far field is known to be smaller by a factor $\sim(a/\lambda)^2$ (where a is a typical dimension of the source) with respect to a dipolar source of comparable size.

It is worth noting that 2D dipoles have a few differences with 3D ones in their expressions of the near and far fields. For a 2D TM dipole $\vec{p}$ in the plane, the magnetic ($\vec{H}_\text{nf}$) and electric ($\vec{E}_\text{nf}$) fields in the near (bound) field at distance r in the direction along $\vec{n}$ read

$$\vec{H}_\text{nf} = \frac{\text{i}\omega}{2\pi r}(\vec{n} \times \vec{p}), \tag{1}$$

and

$$\vec{E}_\text{nf} = \frac{1}{2\pi\epsilon_0 r^2}\left[2(\vec{n}\cdot\vec{p})\vec{n} - \vec{p}\right], \tag{2}$$

where $\omega = 2\pi c/\lambda$ and ϵ_0 is the permittivity of vacuum. The corresponding fields in the radiation region read

$$\vec{H}_\text{rad} = \frac{(1+\text{i})ck^2\text{e}^{\text{i}kr}}{4\sqrt{\pi kr}}(\vec{n} \times \vec{p}), \tag{3}$$

and

$$\vec{E}_{\rm rad} = \frac{(1+{\rm i})k^2 {\rm e}^{{\rm i}kr}}{4\epsilon_0\sqrt{\pi kr}}\left[\vec{p} - (\vec{n}\cdot\vec{p})\vec{n}\right]. \tag{4}$$

The main difference with the 3D case in the radiation zone is the fact that the fields decrease like $1/\sqrt{r}$, to preserve the flux of the Poynting vector and conserve energy. The total power radiated by a 2D dipole can also be evaluated to be

$$P_{\rm 2D} = \frac{\omega^3|\vec{p}|^2}{16\epsilon_0 c^2}. \tag{5}$$

From here we move directly into the effects we want to analyse. In all calculations the metallic objects have the *local* dielectric function given by

$$\epsilon(\lambda) = \epsilon_\infty - \frac{1}{\lambda_p^2(\frac{1}{\lambda^2} + \frac{\rm i}{\Gamma\lambda})}, \tag{6}$$

where $\epsilon_\infty = 4$, $\lambda_p = 141$ nm, $\Gamma = 17\,000$ nm. These parameters provide the best Drude fit for the real optical properties of Ag [40, 41].

4. Selection rule breakdown

Figure 3 shows one of the simplest possible cases where one of the effects we want to discuss is evident; i.e. a finite-size square quadrupole in close proximity with a metallic object. This is a multi-parameter problem. Among the factors one can explore are: (i) the geometry of the metallic object (which changes its intrinsic plasmon resonances); (ii) the separation gap between the emitter and the surface and their relative orientations; (iii) the emission wavelength, and (iv) the distance between dipoles forming the quadrupole. We content ourselves with specific cases that show a particular aspect we want to highlight. Figure 3(b) shows the angular variation of the emission of the quadrupole in two possible situations: (i) the quadrupole on its own, and (ii) the quadrupole in close proximity with the metal. In addition, the figure shows the intensity pattern of a dipole, at the same separation from the surface, built with only two δ-singularities in H_z of the same strength as used for the quadrupole. The angular variation of the far-field emission is presented in a log-polar plot due to the wide range of variation in intensity for the different cases. The calculation is performed for $\lambda = 500$ nm, far from the intrinsic surface plasmon resonance of silver ($\lambda \sim 315$ nm) where most of the radiation emitted by the source goes into non-radiative plasmon excitations. The main two aspects we want to highlight are: (i) the quadrupole emission intensity is enhanced under the close proximity of the metal, and (iii) the angular dependence of the emission becomes almost indistinguishable from a dipolar pattern with only two lobes in the far field. This effect was briefly discussed in [26] using a completely different approach. The underlying reason for this effect can be understood with a hand-waving argument: a small distance of the order of a few ångströms between the two dipoles (forming the finite-size quadrupole) is enough to produce an asymmetry in the coupling to the metal. This asymmetry lifts a small dipolar component from the quadrupole which now dominates in the far field. In terms of the emission from sources close to metals *what matters is not the symmetry and/or multipolarity of the source itself but rather the symmetry of the source + plasmon resonance excitations surrounding it*. This is clearly demonstrated in figure 3 through a simple example. Still, the activated dipolar component of the quadrupole remains small compared to the far-field emission of a single dipole at the same distance, also shown in figure 3(b), by a factor of $\sim 10^4$. If we are modelling the equivalent of Raman allowed/forbidden modes, as explained in the previous section, we would not be able to detect the forbidden frequency with a difference of 10^4 in intensity. However, this is only the simplest example

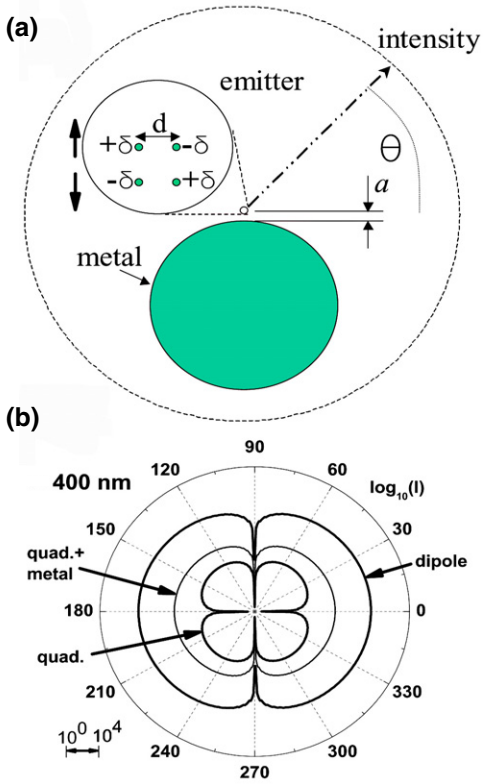

Figure 3. Proximity effects on the emission of a square finite-size quadrupole produced by a cylindrical metallic object. In (a) we show the relevant geometric parameters of the problem: the separation among the δ-singularities in H_z is $d = 1.5$ Å and the distance from the centre of the quadrupole to the surface of the cylinder is $a = 1$ nm. The relative orientation of the equivalent dipoles forming this quadrupole is shown by two small arrows on the left. The cylinder is 50 nm in diameter and with the model dielectric function of Ag given by (6). The polar emission as a function of angle (θ) for the geometry in (a) is plotted in (b) on a log-polar plot for different cases: (i) quadrupole by itself (no metal); (ii) quadrupole in proximity to the metal (as shown in (a)), and (iii) a single dipole at a distance $a = 1$ nm from the metal (for reference). The wavelength is fixed in all cases to be $\lambda = 500$ nm. The emission of the quadrupole is transformed into a dipole-like pattern (as seen by its angular dependence) with a much larger intensity due to the presence of the metal.

of dipole activation from a multipole. Moreover we only consider here the asymmetry in the emission process and a comparable effect is expected in the excitation for a scattering process in general. In more complicated metallic structures (dimers, clusters, etc), where both field enhancements and field gradients can be much larger, it is possible to activate quadrupoles to emit intensities which become comparable to pure dipolar emission from the same place. The whole process is linked to the question of *how large the field gradients can be in a specific metallic structure over small distances of order of molecular sizes to lift some of the dipolar components of a finite-size quadrupole and avoid far-field cancellation among them.*

This is then directly linked to the next aspect we want to discuss in figure 4, which is the extreme sensitivity of the emitting pattern to position. A line quadrupole (I_L) is created by three δ-singularities in H_z as in figure 1(a). The singularities are separated by 1.5 Å (a typical molecular bond length). The quadrupole is equivalent to two out-of-phase dipoles polarized

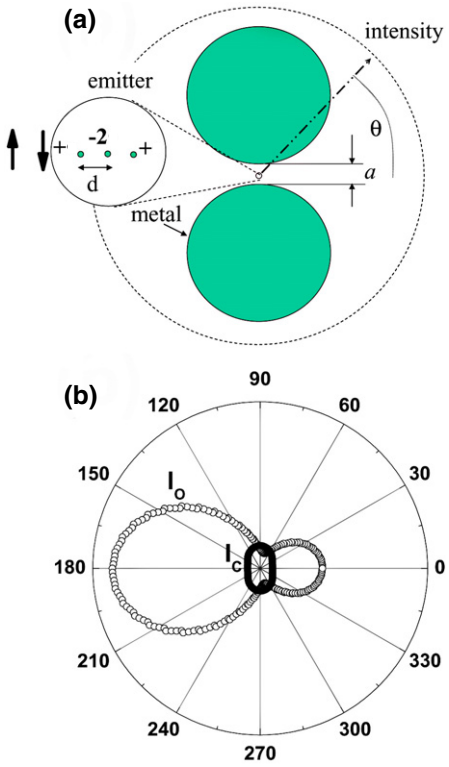

Figure 4. Sensitivity of the emission of a line quadrupole to position. (a) Basic geometry: two 50 nm Ag cylinders separated by a 2 nm gap with a line quadrupole created by three singularities separated by $d = 1.5$ Å (see figure 2(a)). As in figure 3, the two small arrows on the left represent the relative orientation of the two equivalent dipoles forming this quadrupole. The angular dependence of the radiation pattern is evaluated by the flux of the Poynting vector across the circular boundary depicted in the figure as a function of θ. In (b) the patterns for a perfectly centred quadrupole (I_c) and one off-centre (I_O) by 1 nm to the right are shown for an emission wavelength of $\lambda = 500$ nm. Note the asymmetry (focusing) of the emission towards the left-hand side.

along y and separated by 1.5 Å along x; i.e. it can represent a Raman forbidden emission from a molecule. We calculate the emission in two possible cases: (i) the quadrupole is fixed exactly at the centre between the two metallic objects, and (ii) the centre of the quadrupole is shifted from the centre by 1 nm to the right. As before, the angular dependence of the radiation pattern in the far field is calculated in figure 4(b) by evaluating the flux of the Poynting vector across a circular boundary encircling the structure. Figure 4(b) shows the comparison between the emission in the two situations. The sensitivity of the emission pattern to small changes in position is obvious from the figure not only in the intensity but also in the angular distribution. Note how in the second case the radiation is predominantly emitted in one direction, a phenomenon normally seen in antennae. This is achieved by a shift in the position of the quadrupole which is comparable (∼1 nm) to typical molecular dimensions.

5. Radiation funnelling

The phenomenon of radiation funnelling in metallic nanostructures has only been recently studied in the framework of spontaneous emission [42]. Figure 5 shows a streamline plot for

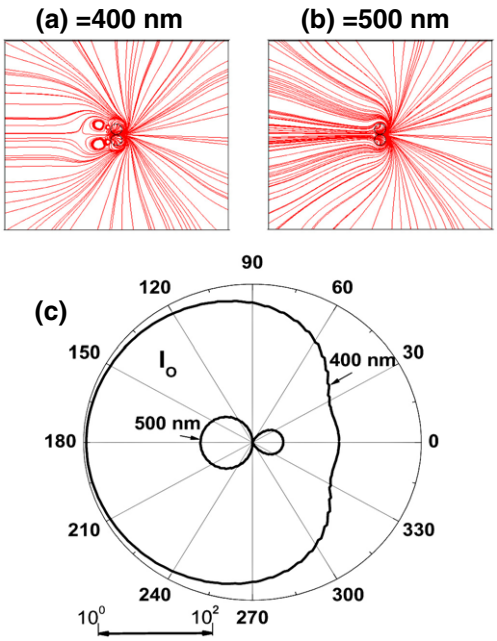

Figure 5. Streamline plots of the Poynting vector flux for the off-axis quadrupole (I_O) in figure 4 at two different wavelengths $\lambda = 400$ nm (a), and 500 nm (b). The amount of focusing in one direction and the details of the angular redistribution depend on λ due to the wavelength dependence of the metal optical properties and the different couplings to plasmon resonances. In (c) the angular dependence of the emission intensity at 400 and 500 nm are shown on a log-polar plot. The intensity emission at 400 nm is $\sim$10 times larger at 180° than at 0°.

the flux of the Poynting vector at two different wavelengths (400 and 500 nm) for the off-centre quadrupole in figure 4. The total intensity of the radiation is different at the two wavelengths (due to the different couplings with the collective plasmon resonances of the structure) but we want to concentrate specifically on the asymmetries of the emission which are evident from the plots in figure 5. Even in a simple structure like this (dimer), which can model many of the situations found in real SERS active media, a substantial amount of redistribution of the energy as a function of angle happens. The funnelling of radiation along specific directions is *not* a property of quadrupolar emission (of particular interest in this paper) but rather a general property of dipolar emission whether on its own or activated from higher-order multipoles through field inhomogeneities. One of the simplest possible examples of this effect is shown explicitly in figure 6, where the emission of a pure dipole in close proximity to a single metallic cylinder is shown for two wavelengths. Note that not only the radiation is more focused in one direction than the other but also the emission pattern lack the zeros (in the direction along the dipole axis) of a normal dipolar emission. A complete separate study could only concentrate on the different angular distributions of the radiation as a function of wavelength and the specific position of the probe for varying types of geometries. It suffices to say for our purposes here, however, that *funnelling* seems to be the rule rather the exception and that this effect can have an additional contribution to the enhancement factors obtained in techniques like SERS. Figures 5 and 6 also show the relative intensity and angular dependence of the radiation at the same wavelengths. For the quadrupole in figure 5 at 400 nm the intensity is ten times larger along 180° than along 0°. This is only *one* simple example of the unlimited number of geometries

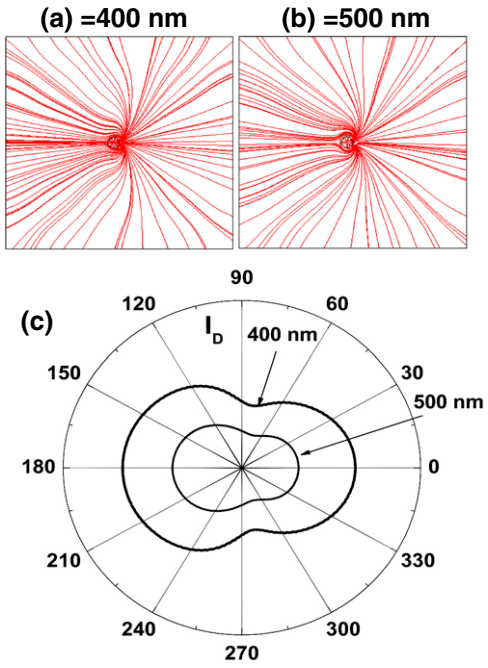

Figure 6. One of the simplest examples of *radiation funnelling* is for a single isolated dipole (polarized in the vertical direction) in close proximity (1 nm from the surface of the right-hand side) to a single Ag cylinder (50 nm diameter). The streamline plots of the Poynting vector are shown in (a) and (b) while the angular pattern of intensity at the two different wavelengths is shown in (c). The *funnelling* effect is not as dramatic as for a dimer (figure 5) but can be readily seen. Note also that the emission pattern lacks the normal zeroes in intensity (along the axis of the dipole) normally seen in free space.

and probe configurations that can be chosen. In general, large field enhancements and narrow angular emission can coexists simultaneously in more complex metallic structures. A few consequences of these phenomena are discussed in the next section.

6. Discussion and conclusions

Having presented the main effects we want to highlight, we discuss in this section their relevance and possible connection to experimentally observed phenomena. Since we introduced the concept of local-field monitoring via a molecular probe using the example of SERS, we shall concentrate on SERS-related phenomena in this section, even though the underlying physics is by no means restricted to it.

The enhancements of the emission in the presence of metallic structures by surface plasmon excitations has been the subject of intense research for a long time in SERS [15, 16]; we shall not dwell on this specific topic, accordingly, except in the relative comparison of dipolar versus quadrupolar emission from the same place in specific cases. The subject of interest here is then not the absolute total enhancement but rather the relative intensity of emission of dipoles versus quadrupoles which are localized within the same (small) local volume. We avoid, consequently, the discussion of the issue of total enhancements and Raman cross sections under SERS conditions. In terms of intensity, figure 3 showed already an example where the emission of a quadrupole can become larger than the normal emission by a

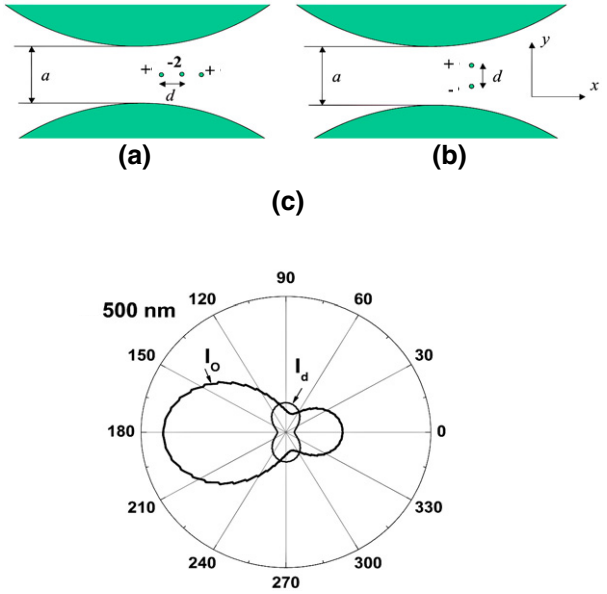

Figure 7. Comparison between quadrupolar (a) and dipolar (b) emission from the same local environment. In (a) and (b) we show the geometries which consist of two cylinders separated by 2 nm (not drawn to scale) and a quadrupolar or dipolar source in (a) and (b), respectively. The dipole in (b) is made of two δ-singularities in H_z (normal to the page) which are off-centre (to the right) with respect to the cylinders by 1 nm. The two singularities are separated by 1.5 Å and represent an electric dipole in the plane polarized along x. In (a), three singularities in H_z model two dipoles separated by 1.5 Å polarized along y and emitting out of phase with each other. The distance d is again 1.5 Å and the central singularity is off-axis by 1 nm as before. The angular dependence of the radiation is shown in (c) on a linear-polar plot. I_O and I_d represent the radiation of the off-centre quadrupole and dipole, respectively at $\lambda = 500$ nm. At 90° (270°) the radiation of the two configurations is comparable while at 180° is completely dominated by the quadrupole.

simple proximity to a metallic object. Nevertheless, the quadrupole emission is in this case still smaller (by another factor of 10^4) with respect to a pure dipolar emission from the same place. It is understood throughout that this is the emission of a dipole with the same strength as the ones used for the quadrupole geometry.

Figure 7 shows a counterexample in a slightly more complicated case. Here we compare the quadrupole emission at 500 nm for a line quadrupole as in figure 4 with the dipole emission (created by two singularities of the same strength and localized within the same volume). The spatial configuration of the singularities representing both cases is depicted in figures 7(a) and (b). Figure 7(c) shows that, depending on the scattering direction we are looking at, we can detect a signal in which (i) the dipolar and quadrupolar emissions have comparable magnitudes or (ii) the quadrupolar emission (a normally Raman forbidden case) dominates. The two configurations in figures 7(a) and (b) could certainly represent two vibrational modes confined within a radius comparable to the size of a molecule and emitting with different symmetries.

We discuss in what follows the possible relevance of the phenomena highlighted here for real spectroscopic application using again the case of SERS as an example.

- The possible breakdown of Raman selection rules based on a purely electromagnetic contribution is quite clear from the examples displayed in this paper, in particular figure 7. SERS is plagued with selection rule breakdowns and fluctuations of signals showing spectral components which are not normally seen under standard scattering conditions; this

was partly discussed in [26]. However, the Raman cross section under SERS conditions is a substantially more complicated phenomenon than the simple emission studied here. In other words, the fact that a field inhomogeneity can lift a Raman selection rule does not mean in general that the signal will be seen. In addition, SERS fluctuations are known to be affected by the environment (in particular the presence of oxygen). A full explanation of this effect is still missing. Notwithstanding, the results in this paper show that Raman selection rule breakdowns could have a contribution, at least, from a purely electromagnetic component. The fluctuations themselves cannot be explained in electromagnetic terms and their most probable origin is in molecular motions and rearrangements of the atoms on a $\sim$1 nm length scale over time scales of the order of $\sim$ ms. The results in this paper, however, show how—for a fixed atomic configuration—Raman inactive modes can be seen (if all the other conditions on the Raman cross section are fulfilled), and how the signals can fluctuate and appear/disappear due to the extreme sensitivity to position on molecular length scales.

- The redirection or *funnelling* of radiated energy is an interesting effect which has not received much attention in terms of possible spectroscopic manifestations. We see this particular aspect to be complementary to the interest in emission of sources in close proximity to metals for near-field imaging, and certainly more significant for spectroscopic applications. The influence of a metallic environment on the angular emission of a single molecule has even been observed experimentally [44], but the full implications for spectroscopic applications remain largely unexplored. The issue of funnelling highlights one of the problems still under discussion in SERS scattering cross sections. There are two main lines of thought in this respect. A good fraction of the work has been interpreted under the assumption that *both* the incident and the scattered (Stokes or anti-Stokes) fields are enhanced in SERS conditions. Under this assumption, and in the limit of small Raman shifts, the scattering cross section is proportional to the fourth power of the field [16]. This point of view implies an intrinsic enhancement of the Raman cross section along the lines of modified spontaneous emission [43]. However, other conceptually different versions of how the scattering process occurs have been put forward. Moskovits *et al* [45, 46] take a different point of view on the SERS enhancement where the process is also separated into an incident excitation stage and a reemission process. In this second view, the 'enhancement' in the Stokes field comes from the radiation being re-emitted preferentially along certain directions. It is not accordingly a modification of the Raman cross section at the Stokes field that contributes to the scattering intensity but rather a redistribution of the radiation produced by the interaction with the plasmons. This paper shows that, in fact, the two properties are not mutually exclusive and they can be operating together in most experimental situations of interest where huge enhancements are monitored. Large enhancement and energy funnelling together could be behind some of the largest SERS enhancement seen in certain experimental situations. The examples shown here are rich enough to show hints of enhancement and energy funnelling coexisting with each other, selection rule breakdowns, and emission symmetry changes in the far field. The energy funnelling effect by itself, however, cannot account for the total cross section enhancement seen in SERS. All the examples we have investigated suggest that the latter can account for a factor between 10^1 and 10^2 and therefore it would be insufficient to explain the experimental enhancements without the intrinsic modification of the cross section.

In closing, we have highlighted several aspects of the electromagnetic emission of multipoles in close proximity to metal nanostructures which we believe are playing a role in many spectroscopic applications involving the optical properties of plasmons. The particular

effects of Raman selection rule breakdowns under SERS conditions and energy *funnelling* in the far field have been highlighted and demonstrated. The latter, in particular, would have an additional contribution to the SERS cross section in the reemission of the Stokes field and requires careful consideration for individual geometries.

Acknowledgments

PGE acknowledges partial support for this work by the Engineering and Physical Sciences Research Council (EPSRC) of the UK under grant GR/T06124. We are indebted to Manuel Cardona (Max-Planck Institute für Festkörperforschung), Lesley F Cohen (Imperial College) and Robert C Maher (Imperial College) for useful discussions on SERS-related topics.

References

[1] John S 1987 *Phys. Rev. Lett.* **58** 2486
[2] Busch K and John S 1998 *Phys. Rev.* E **58** 3896
[3] Sheng P (ed) 1990 *Scattering and Localization of Classical Waves in Random Media* (*Series on Directions in Modern Condensed Matter Physics*) (Singapore: World Scientific)
[4] Apalkov V M, Raikh M E and Shapiro B 2002 *Phys. Rev. Lett.* **89** 016802
[5] Kovalev E G, Künzner N, Diener J, Koch F and Fujii M 2002 *Phys. Rev. Lett.* **89** 267401
[6] Stockman M I 2000 *Phys. Rev. Lett.* **84** 1011
[7] Zayats A V, Smolyaninov I I and Maraudin A A 2005 *Phys. Rep.* **408** 131
[8] Xu H and Käll M 2002 *Phys. Rev. Lett.* **89** 246802
[9] Arnoldus H F 2004 *Surf. Sci.* **571** 173
[10] Larkin I A, Stockmann M I, Achermann M and Klimov V I 2004 *Phys. Rev.* B **69** 121403
[11] Shalaev V M 1996 *Phys. Rep.* **272** 61
[12] Fuchs R and Barrera R G 1981 *Phys. Rev.* B **24** 2940
[13] Ford G W and Weber W H 1984 *Phys. Rep.* **113** 195
[14] Kreiter M, Neumann T, Mittler S, Knoll W and Sambles J R 2001 *Phys. Rev.* B **64** 075406
[15] Moskovits M 1985 *Rev. Mod. Phys.* **57** 783
[16] Otto A 1984 *Light Scattering in Solids* ed M Cardona and G Güntherodt (Berlin: Springer) p 289
[17] Pendry J B 2000 *Phys. Rev. Lett.* **85** 3966
[18] Pendry J B 2001 *Phys. World* **14** (9) 47
[19] Williams J M 2001 *Phys. Rev. Lett.* **87** 249703
Pendry J B 2001 *Phys. Rev. Lett.* **87** 249704
[20] Valanju P M, Walser R M and Valanju A P 2002 *Phys. Rev. Lett.* **88** 187401
Pendry J B and Smith D R 2003 *Phys. Rev. Lett.* **90** 029703
[21] Garcia N and Nieto-Vesperinas M 2002 *Phys. Rev. Lett.* **88** 207403
Pendry J B 2003 *Phys. Rev. Lett.* **91** 099701
[22] Melville D O S, Blaikie R J and Wolf C R 2004 *Appl. Phys. Lett.* **84** 4403
[23] Pendry J B and Ramakrishna S A 2002 *J. Phys.: Condens. Matter* **14** 8463
[24] Merlin R 2004 *Appl. Phys. Lett.* **84** 1290
[25] Webb K J, Yang M, Ward D W and Nelson K A 2004 *Phys. Rev.* E **70** 035602
[26] Etchegoin P G, Maher R C and Cohen L F 2004 *New J. Phys.* **6** 142
[27] Yu P Y and Cardona M 1999 *Fundamentals of Semiconductors* 2nd edn (Berlin: Springer) p 362
[28] Cardona M and Güntherodt G (ed) 1982 *Light Scattering in Solids II* (Berlin: Springer)
[29] Brüesch P (ed) 1986 *Phonons: Theory and Experiments II* (Berlin: Springer)
[30] Volkenstein M V 1941 *C. R. Acad. Sci. URSS* **30** 791
[31] Purcell E M and Pennypacker C R 1973 *Astrophys. J.* **186** 705
[32] Félidj N, Aubard J and Lévi G 1999 *J. Chem. Phys.* **111** 1195
[33] Yang W H, Schatz G C and van Duyne R P 1995 *J. Chem. Phys.* **103** 869
[34] Goodman J J, Draine B T and Flatau P J 1991 *Opt. Lett.* **16** 1198
[35] Zienkiewicz O C and Zhu J Z 1991 *Int. J. Numer. Methods Eng.* **32** 783
[36] Gyimóthy Sz and Sebestyén I 1997 *Applied Electromagnetics and Computational Technology* ed H Tsuboi and I Sebestyén (Amsterdam: IOS Press) p 207

[37] Zienkiewicz O C and Taylor R L 1989 *The Finite Element Method* vol 1 (New York: McGraw-Hill) p 436
[38] Jackson J D 1998 *Classical Electrodynamics* (New York: Wiley)
[39] FEMLAB v3.1 (see footnote 1) *User's Guide Application Manual*
[40] Palik E D (ed) 1998 *Handbook of Optical Constants of Solids, III* (New York: Academic)
[41] Rojas R and Claro F 1993 *J. Chem. Phys.* **98** 998
[42] Blanco L A and García de Abajo F J 2004 *Phys. Rev.* B **69** 205414
[43] Le Ru E C and Etchegoin P G, unpublished
[44] Gersen H, García-Parajó M F, Novotny L, Veerman J A, Kuipers L and van Hulst N F 2000 *Phys. Rev. Lett.* **85** 5312
[45] Haslett T L, Tay L and Moskovits M 2000 *J. Chem. Phys.* **113** 1641
[46] Moskovits M, Tay L L, Yang J and Haslett T 2002 *Top. Appl. Phys.* **82** 215